

Characterization of the thermo-mechanical properties of p-type (MnSi1.77) and n-type (Mg2Si0.6Sn0.4) thermoelectric materials

Mahdi Mejri, Yohann Thimont, Benoît Malard, Claude Estournès

▶ **To cite this version:**

Mahdi Mejri, Yohann Thimont, Benoît Malard, Claude Estournès. Characterization of the thermo-mechanical properties of p-type (MnSi1.77) and n-type (Mg2Si0.6Sn0.4) thermoelectric materials. Scripta Materialia, 2019, 172, pp.28-32. 10.1016/j.scriptamat.2019.06.037 . hal-02186148

HAL Id: hal-02186148
https://hal.science/hal-02186148

Submitted on 17 Jul 2019

HAL is a multi-disciplinary open access archive for the deposit and dissemination of scientific research documents, whether they are published or not. The documents may come from teaching and research institutions in France or abroad, or from public or private research centers.

L'archive ouverte pluridisciplinaire **HAL**, est destinée au dépôt et à la diffusion de documents scientifiques de niveau recherche, publiés ou non, émanant des établissements d'enseignement et de recherche français ou étrangers, des laboratoires publics ou privés.

OATAO
Open Archive Toulouse Archive Ouverte

Open Archive Toulouse Archive Ouverte (OATAO)

OATAO is an open access repository that collects the work of Toulouse researchers and makes it freely available over the web where possible

This is an author's version published in: http://oatao.univ-toulouse.fr/24127

Official URL: https://doi.org/10.1016/j.scriptamat.2019.06.037

To cite this version:

Mejri, Mahdi and Thimont, Yohann and Malard, Benoît and Estournès, Claude *Characterization of the thermo-mechanical properties of p-type (MnSi1.77) and n-type (Mg2Si0.6Sn0.4) thermoelectric materials.* (2019) Scripta Materialia, 172. 28-32. ISSN 1359-6462

Any correspondence concerning this service should be sent to the repository administrator: tech-oatao@listes-diff.inp-toulouse.fr

Characterization of the thermo-mechanical properties of p-type ($MnSi_{1.77}$) and n-type ($Mg_2Si_{0.6}Sn_{0.4}$) thermoelectric materials

M. Mejri [a], Y. Thimont [a], B. Malard [b], C. Estournès [a,*]

[a] CIRIMAT, Université de Toulouse, CNRS, Université Toulouse 3 - Paul Sabatier, 118 Route de Narbonne, 31062 Toulouse cedex 9, France
[b] CIRIMAT, Université de Toulouse, CNRS, INP- ENSIACET, 4 allée Emile Monso BP44362, 31030 Toulouse cedex 4, France

ARTICLE INFO

Keywords:
Silicide
Hardness
Toughness
Young's modulus
Thermal expansion coefficient
Emissivity
Spark plasma sintering

ABSTRACT

The thermoelectric generators reliability is highly sensitive to the materials they are made off. This work aims to characterize the structure, microstructure, emissivity and thermo-mechanical properties of p-type ($MnSi_{1.77}$) and n-type ($Mg_2Si_{0.6}Sn_{0.4}$) highly promising thermoelectric materials. In particular, the temperature dependence of the Young's modulus, evaluated by impulse excitation technique, shows for both materials values higher than those reported in literature. Fracture toughness measured by both single edge notched beam and indentation methods exhibits similar values to those reported in the literature. Micro-indentation measurements reveal that the hardness values of the $MnSi_{1.77}$ are significantly higher than the $Mg_2Si_{0.6}Sn_{0.4}$ one.

A thermoelectric generator (TEG) is a static and autonomous system that converts thermal energy into electrical energy and vice-versa. TEG are constituted by pairs of n-type and p-type thermoelectric materials (also called legs) which are electrically connected in series and thermally in parallel. These thermoelectric materials are put in sandwich between two metallized ceramic plates (π geometry) and brazed on electrical tracks which provide a good electrical and thermal transfer and insure a high mechanical cohesion of the whole set [1].

The thermoelectricity markets are in full development with the growing interest in the recovery of dissipated thermal energy and temperature management of electronic components [2–6]. Industrial needs are mainly limited to a low (0–250 °C) and medium (250–500 °C) temperature ranges [7,8]. For low temperatures, the devices available on the market are based on bismuth telluride alloys. However, for medium temperatures range, to this day, very few TEG modules are commercialized while numerous industrial applications dissipate thermal waste in this range of temperatures [2,3,9]. Due to their good thermoelectric performances, some compounds were identified for medium temperatures applications, as silicides [10–15] or skutterudites [16] which are under development. However, crucial challenges remain to be solved in terms of i) robustness (mechanical), ii) chemical stability, iii) toxicity of the materials, iv) fabrication cost and v) mass production capacity before they could be put on the market.

* Corresponding author.
E-mail address: estournes@chimie.ups-tlse.fr (C. Estournès).

Degenerated semiconductors, including $Mg_2Si_{1-x}Sn_x$ [11,16–19] and $MnSi_{1.77}$ also called high manganese silicide (HMS) [10–15,19], belong to the family of the most promising thermoelectric materials for medium temperature applications. Mg_2X intermetallic compounds (X = Si, Ge and Sn) and their solid solutions ($Mg_2Si_{1-x}Sn_x$) are high quality thermoelectric candidates [16]. The synthesis of these materials is the subject of several research studies [10–15]. However, in only few of them [11], the characterization of their thermo-mechanical properties have been carried out while for thermoelectric applications their knowledge is crucial to improve the reliability of the generators.

The TEG, usually assembled by brazing, is subjected to temperature cycles of high amplitude, long durations depending on the type of applications (i.e.: automotive, aeronautic…), but also to very important thermal gradients (i.e. hundreds of degree/cm). The reliability of thermoelectric devices is dependent on the cyclic thermal loads they undergo which cause thermo-mechanical stresses at different packaging interfaces due to the diversity of materials used in the manufacture of the system (i.e.: Ag, AlN, Cu, TE materials). This is mainly due to the mismatch of the of thermal expansion coefficients (TEC) between these materials (metallization-substrate/TE materials) [20,21]. In addition, thermoelectric materials are brittle (low toughness) with restricted plastic accommodation that limits their use, the difference in stiffness and TEC of these materials can generate stresses at the interfaces of the TE module, which can lead to cracks. The presence of the latter's in the module induces an increase in thermal and electrical resistances leading to system overheating and its failure [22–24].

https://doi.org/10.1016/j.scriptamat.2019.06.037

Table 1
Mechanical proprieties of $MnSi_{1.77}$ and $Mg_2Si_{0.6}Sn_{0.4}$.

Material	Fracture toughness		Vickers hardness	Thermal expansion coefficient	Young modulus	
	Via SNEB	Via hardness			25 °C	500 °C
	K_{IC} [MPa.m$^{0.5}$]		Hv [GPa]	α [10^{-6} K^{-1}]	E [GPa]	
$MnSi_{1.77}$	2.5 ± 0.3	1.60 ± 0.15	16.0 ± 1.1	12	281	263
$Mg_2Si_{0.6}Sn_{0.4}$	1.0 ± 0.1	0.70 ± 0.15	4.5 ± 0.4	17	90	82

To better optimize TEG's design, it is essential that their thermoelectric materials are both highly-performing and mechanically reliable. In addition to the thermoelectric properties, it is important to know the thermo-mechanical characteristics of thermoelectric materials such as their thermal expansion coefficient (TEC), Young's modulus (E), toughness as well as their hardness to validate their performances and reliability in operating thermoelectric devices. This work aims at characterizing the structure, the microstructure, the emissivity (ε) and thermo-mechanical properties of two promising thermoelectric materials ($Mg_2Si_{0.6}Sn_{0.4}$ and $MnSi_{1.77}$) and comparing them, when they are available, with those reported in the literature.

Our industrial partner HotBlock OnBoard has manufactured legs of two thermoelectric materials of respective composition: $MnSi_{1.77}$ (HMS) and $Mg_2Si_{0.6}Sn_{0.4}$, through the spark plasma sintering (SPS) process [25]. After sintering, the relative density of both materials was measured by the Archimedes. Method. Values of 96% and 99% were obtained for respectively $MnSi_{1.77}$ and $Mg_2Si_{1-x}Sn_x$ indicating that SPS led to fully dense pellets. Then, the latter have been cut by a micro-cutter with a specific lubricant for each of them: water for the $MnSi_{1.77}$ and oil for the $Mg_2Si_{0.6}Sn_{0.4}$ (to protect it against oxidation).

The different crystallographic phases were analyzed by X-ray diffraction using a D4 Endeavor diffractometer ($\lambda_{Cu_{K\alpha 1\&2}} = 1.541$ Å). The microstructures were characterized using a scanning electron microscope JEOL JSM-7100 TTLS LV with an energy dispersive spectroscopy (EDS) detector SDD X-Max 80 mm^2 Oxford Instruments Aztec Energy and an electron backscatter diffraction (EBSD) detector AZtec HKL Advanced Nordlys Nano and an optical microscope NIKON ECLIPSE MA200 (without etching).

TEC analyses were performed on both thermoelectric materials using a Setaram Setsys Evo dilatometer using heating and cooling rates of 5 °C/min. The tests were conducted under argon gas to avoid oxidation. $MnSi_{1.77}$ has undergone two heating cycles with a 3-hour hold at 1050 °C. $Mg_2Si_{0.6}Sn_{0.4}$ has undergone two heating cycles with a 3-hour hold at 600 °C.

The single edge notched beam (SENB) technique [26,27] was used to measure the fracture toughness (K_{IC}) of parallelepipedic samples using relation (1) [27].

$$K_{IC} = \frac{FL}{ab^{\frac{3}{2}}} \frac{3\left(\frac{c}{b}\right)^{\frac{1}{2}}\left[1.99-\left(\frac{c}{b}\right)\left(1-\left(\frac{c}{b}\right)\right)\left(2.15-3.93\frac{c}{b}+2.7\left(\frac{c}{b}\right)^2\right)\right]}{2\left(1+2\frac{c}{b}\right)\left(1-\frac{c}{b}\right)^{\frac{3}{2}}} \quad (1)$$

where F (N) is the maximum load, L (mm) is the span between the two outer supports, a (mm) is the width, b (mm) is the thickness and c (mm) is the size of the notch in the specimen.

Notches were created with a diamond wire saw (200 μm in diameter), their deepness were measured precisely (±0.5 μm) using an optical microscope. The tests (10 specimens for each materials) were conducted on an MTS tensile system equipped with a cell with a capacity of 5 kN. The toughness values via SENB technique (Table 1) were performed with a c/b ratio between 0.46 and 0.55. The SENB tests until failure were performed with a loading speed of 3 mm/min on and a reach of 13 mm.

The micro-indentation was used to measure the Vickers hardness (Hv) of both thermoelectric materials. The tests were carried out using a micro-hardness tester (HM 200 – MITUTOYO) with a square-based pyramidal diamond indenter tip. The indentations were performed on polished surfaces of the samples. The Vickers microhardness of both materials was measured at several charges (0.03 kg, 0.05 kg and 0.1 kg). To determine the mean hardness, a minimum of 10 indents were made at each load. The microhardness is calculated from the applied load P (N) and the length of both diagonal d_1 (mm) and d_2 (mm) of this indentation according to the following relation [28]:

$$Hv = \frac{2P\sin\left(\frac{136}{2}\right)}{d_1 d_2} = 0.1891\frac{P}{d_1 d_2} \quad (2)$$

Through the Vickers indentation tests, toughness is evaluated by the measurement of the length of radial cracks (Fig. 3) formed at the corners of the hardness indentation marks [29,30]. The determination of toughness is then obtained by applying the Charles and Evans' analytical relation (3), which integrates the geometric specifications of the radial crack [31]:

$$K_{IC} = 0.0752\frac{F}{c^{\frac{3}{2}}} \quad (3)$$

where F (N) is the applied force and c (mm) is the average length of the cracks created at the corners of the indentation and measured from its center.

E measurements were conducted by impulse excitation technique (IET) [32–34]. The measurement is based on the theory of the propagation of mechanical waves in solids. A pulse is given on beam or cylinder shape material with a small hammer. The sound waves propagate in the material, as a result of this shock, the sound is listened with a microphone. While the material vibrates at its resonance frequency, the measured frequency will be a characteristic of the mechanical support points (tensile or torsion) of the specimen, its geometry and its elastic properties. A series of measurements were made with an appropriate experimental set-up (fundamental flexure or torsion mode) for each

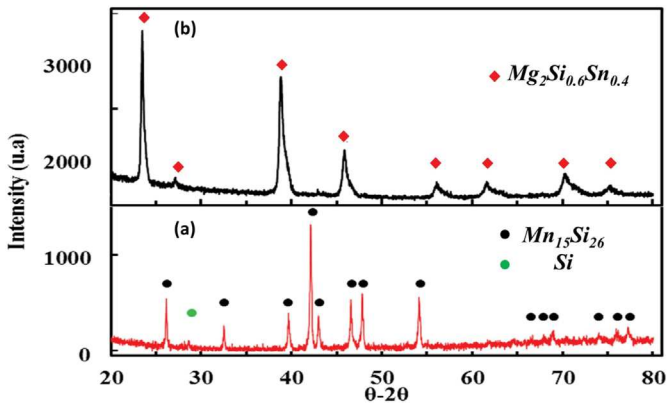


Fig. 1. X-ray diffraction patterns for: a) $MnSi_{1.77}$ and b) $Mg_2Si_{0.6}Sn_{0.4}$.

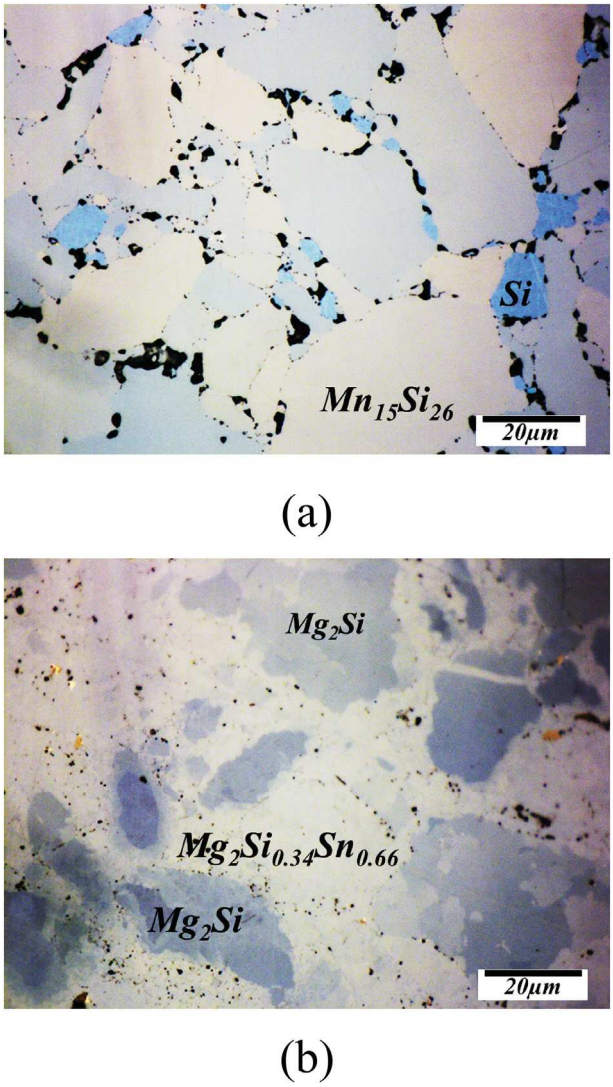


Fig. 2. Optical micrographs of: a) $MnSi_{1.77}$ and b) $Mg_2Si_{0.6}Sn_{0.4}$. (For interpretation of the references to color in this figure, the reader is referred to the web version of this article.)

sample for temperatures between 25 °C and 500 °C with a heating rate of 2 °C/min. The temperature is expressed in °C and the E is given in GPa. E measurements in temperature using this method were carried out at Aurock company according to ASTM E 1876, ISO 12680-1, ENV 843-2 corresponding to the first mode of vibration.

Emissivity of both materials was measured at 60 °C thank to a AEL Device Service emissiometer with an accuracy of (+/− 0.01).

The XRD patterns of $MnSi_{1.77}$ and $Mg_2Si_{0.6}Sn_{0.4}$ (Fig. 1) obtained on the sintered samples, after baseline subtraction, have shown intense and fine peaks indicating a good crystallization of elaborated materials. On one hand, pattern analysis of $MnSi_{1.77}$ has revealed the presence of the major phase $Mn_{15}Si_{26}$ which crystalized in the tetragonal system (JCPDS file n°00-020-0724) with some weak peaks of the silicon phase (JCPDS file n°00-027-1402). On The other hand, concerning the $Mg_2Si_{0.6}Sn_{0.4}$ material, the $Mg_2Sn_{0.6}Si_{0.4}$ phase crystallized in the cubic system (JCPDS file n°01-077-2914) has been identified on the X-ray pattern. For this compound, the asymmetric form of the diffraction lines is due to the presence of several families of the same phase but with different lattice parameters, sizes and micro-deformation of crystallites.

The microstructures of the investigated materials are illustrated in the Fig. 2. The microstructure of $MnSi_{1.77}$ (Fig. 2a) is mainly composed of a gray matrix (HMS saturated in Manganese) in which minor silicon inclusions (blue phase) are located at the grains boundaries. Due to the manufacturing process and the dispersion of the powder grain size (20–50 μm), some voids (black spots) are also located at the grains boundaries in agreement with the relative density (96%) reported previously. The size of the $MnSi_{1.77}$ grains measured by EBSD analysis on sintered samples varies from 2 to 67 μm. The average grain size is 6 μm (statistic on 2495 grains). For $Mg_2Si_{0.6}Sn_{0.4}$ material microstructure (Fig. 2b), it can be noted the presence of two phases homogeneously distributed in the material. On the basis of EDS analysis, it is deduced that the gray phase corresponds to the Mg_2Si and the white phase corresponds to the $Mg_2Si_{0.6}Sn_{0.4}$ matrix. Here again the microstructure is in agreement with the relative density measurement (99%) since no significant porosity is observed, $Mg_2Si_{0.6}Sn_{0.4}$ has a higher relative density compared to $MnSi_{1.77}$. The size of the $Mg_2Si_{0.6}Sn_{0.4}$ grains measured by EBSD analysis after sintering varies between 3 and 46 μm. The average grain size is 7 μm (statistic on 4521 grains).

The average values of the Vickers hardness (load of 0.1 kg for 10 s) at room temperature of $MnSi_{1.77}$ and $Mg_2Si_{0.6}Sn_{0.4}$ are 15 ± 1 GPa and 4.20 ± 0.35 GPa respectively, (Table 1). $MnSi_{1.77}$ and $Mg_2Si_{0.6}Sn_{0.4}$ have a higher hardness than those found in the literature (HMS: 11.85 GPa,

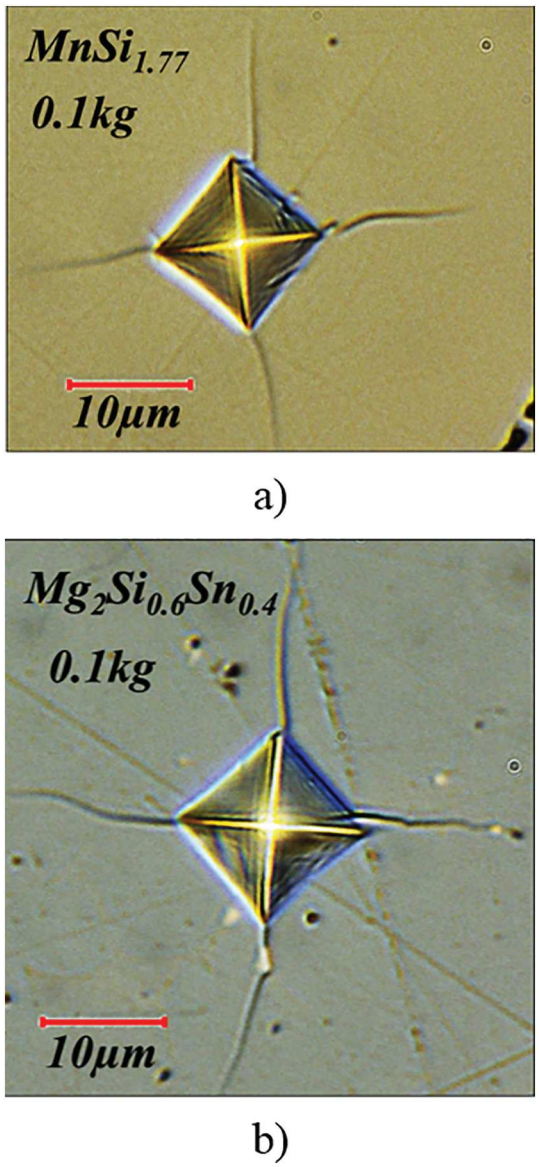


Fig. 3. Vickers microhardness indentations of a) $MnSi_{1.77}$ and b) $Mg_2Si_{0.6}Sn_{0.4}$.

$Mg_2Si_{1-x}Sn_x$: 3.54 GPa, load of 1 Kg for 10 s) [11]. This can be explained by the fact that the hardness of a such material is highly dependent on its microstructure, silicon content and stress state of each material after shaping. In addition, the use of heavy loads for indentation favors the generation of cracks (dissipated energy) which reduces the measured Vickers hardness of the materials.

When the indenter penetrates, visible cracks on the surface of the sample ($MnSi_{1.77}$ and $Mg_2Si_{0.6}Sn_{0.4}$) are created and extend from the center of the indentation through its corners (Fig. 3). Once initiated, these cracks propagate under residual contact stresses and this propagation stops when the stress intensity factor at the crack base becomes equal or lower to the toughness of the material.

In the present work, two techniques were used to evaluate the fracture toughness of the both materials. It is known that the toughness value depends on the nature of materials investigated but also to the chosen technique used to evaluate it [27]. The toughness values obtained from indentation test using Eq. (3) are reported in Table 1. The toughness values of both thermoelectric materials were also determined from SENB technique using Eq. (1). The average toughness values of $MnSi_{1.77}$ using the SENB technique and indentation fracture test are 2.5 ± 0.3 MPa.m$^{0.5}$ and 1.60 ± 0.15 MPa.m$^{0.5}$ respectively. The average toughness values of $Mg_2Si_{0.6}Sn_{0.4}$ using the SENB technique and indentation fracture test are 1.0 ± 0.1 MPa.m$^{0.5}$ and 0.70 ± 0.15 MPa.m$^{0.5}$ respectively. The values found are close to those found in the literature (HMS: 1.63 MPa.m$^{0.5}$, $Mg_2Si_{1-x}Sn_x$: 0.99 MPa.m$^{0.5}$) [11]. Both materials have very low toughness values which could have detrimental consequences during the TEG device assembling and for their reliability. The application of heavy loads during the brazing step can initiate and promote the propagation of lateral cracks that can cause flaking by opening onto the surface of the specimen.

The evolution of the TEC of $MnSi_{1.77}$ and $Mg_2Si_{0.6}Sn_{0.4}$ are reported in Fig. 4a. For the $MnSi_{1.77}$, we have noticed that the overall shape of the cycle during heating is almost the same (around 12 10^{-6} K^{-1}). In all tests, the material underwent substantial densification after 1 h of holding at 1050 °C. $Mg_2Si_{0.6}Sn_{0.4}$ is stable for both heaters in the room and 600 °C. The TEC mean value of $Mg_2Si_{0.6}Sn_{0.4}$ (17 10^{-6} K^{-1}) is higher than that of $MnSi_{1.77}$ (12 10^{-6} K^{-1}). This difference between the two thermoelectric materials generates mechanical stresses and induces an asymmetric global thermal expansion during the operation of TEG.

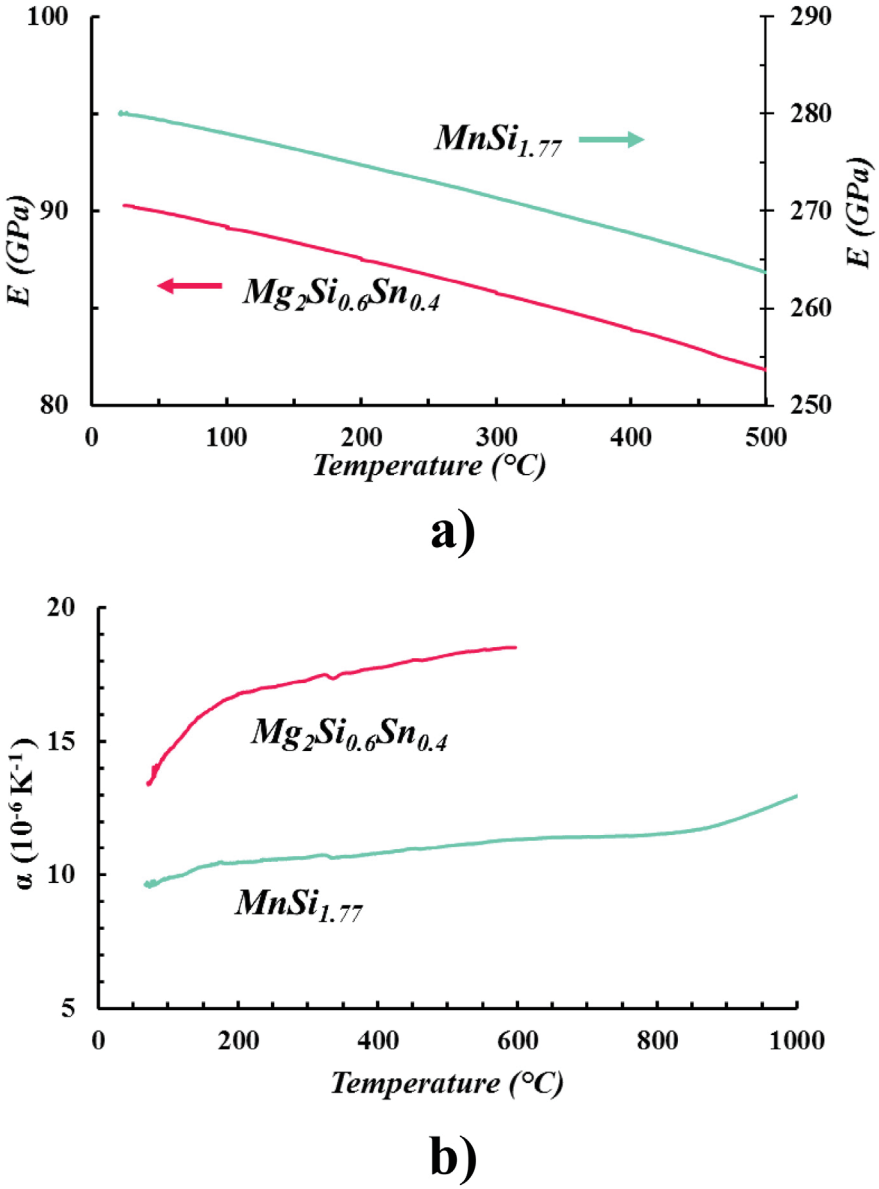


Fig. 4. (a) Thermal expansion coefficient vs temperature and (b) Young's modulus vs temperature of $MnSi_{1.77}$ and $Mg_2Si_{0.6}Sn_{0.4}$.

In the present study, the mean values of Young's modulus at room temperature of $MnSi_{1.77}$ and $Mg_2Si_{0.6}Sn_{0.4}$ are 281 ± 2 GPa and 90 ± 1 GPa respectively. The elastic modulus obtained for $Mg_2Si_{0.6}Sn_{0.4}$ is in good agreement with the values given in the literature (83 ± 25 GPa) [5]. On the other hand, Young's modulus obtained for $MnSi_{1.77}$ is higher than the values given in the literature (160 ± 30 GPa) [5]. Their evolution with temperature is also reported in Fig. 4b. A monotonous decrease is noted when the temperature increases up to 500 °C for both materials. Young's modulus of $MnSi_{1.77}$ decreases from 281 GPa at 25 °C to 263 GPa at 500 °C and from 90 GPa at 25 °C to 82 GPa at 500 °C for $Mg_2Si_{0.6}Sn_{0.4}$. Several studies have revealed the temperature dependence of Young's modulus via IET [33,34]. Depending on the authors, Arrhenius or polynomial law are used to describe their temperature dependence. It depends on the thermal behavior of the sample. Here, the evolution of Young's modulus of $MnSi_{1.77}$ and $Mg_2Si_{0.6}Sn_{0.4}$ as a function of temperature can be well fitted (R^2) using three order polynomial laws; thus their behavior law can be described by the relations (4) and (5).

$$MnSi_{1.77} : E = 280.70 - 2610^{-3}T - 2010^{-6}T^2 + 610^{-9}T^3 \quad (4)$$

$$Mg_2Si_{0.6}Sn_{0.4} : E = 90.66 - 14.910^{-3}T - 310^{-6}T^2 - 410^{-9}T^3 \quad (5)$$

Finally, the measured emissivity values are 0.60 and 0.70 for $MnSi_{1.77}$ and $Mg_2Si_{0.6}Sn_{0.4}$ respectively.

Although considerable researches have been carried out to investigate the synthesis and thermoelectric properties of $MnSi_{1.77}$ and $Mg_2Si_{0.6}Sn_{0.4}$, very little information is available in the literature regarding their thermomechanical properties (TEC, Hv, K_{1C}). In this paper, we fill this gap investigating the mechanical properties of as well as the structure, microstructure of $MnSi_{1.77}$ and $Mg_2Si_{0.6}Sn_{0.4}$. In particular, to the best of our knowledge, for the first time the thermal dependence of Young modulus of both materials has been determined using impulse excitation technique and a behavior law has been proposed.

TEG modules of 24 legs have already been produced exhibiting interesting performances (Power max delivered = ~1 W/cm^2 with a yield of ~4.5% for T_{hot} = 450 °C and T_{low} = 50 °C). All the properties measured in this work will be very helpful to supply a numerical model to simulate the thermo-mechanical behavior of the TEG and to optimize their design and performances.

Acknowledgment

This Project is funded by the French National Research Agency (ANR-16-CE05-0012-03). Authors would like to thank the partners from the company HotBlock OnBoard for the supply of thermoelectric materials.

References

[1] J. Yang, T. Caillat, MRS Bull. 31 (2006) 224–229.
[2] L.E. Bell, Science 321 (2008) 1457–1461.
[3] T. Mori, JOM 68 (2016) 2673–2679.
[4] G.J. Snyder, E.S. Toberer, Nat. Mater. 7 (2008) 105–114.
[5] C. Dagdeviren, Z. Li, Z.L. Wang, Annu. Rev. Biomed. Eng. 19 (2017) 85–108.
[6] T. Mori, S. Priya, MRS Bull. 43 (2018) 176–180.
[7] D. Champier, Energy Convers. Manag. 140 (2017) 167–181.
[8] H.J. Goldsmid, Materials 7 (2014) 2577–2592.
[9] I. Petsagkourakis, K. Tybrandt, X. Crispin, I. Ohkubo, N. Satoh, T. Mori, Sci. Technol. Adv. Mater. 19 (2018) 836–862.
[10] D.-K. Shin, K.-W. Jang, S.-C. Ur, I.-H. Kim, J. Electron. Mater. 42 (2013) 1756–1761.
[11] Y. Gelbstein, J. Tunbridge, R. Dixon, M.J. Reece, H. Ning, R. Gilchrist, R. Summers, I. Agote, M.A. Lagos, K. Simpson, C. Rouaud, P. Feulner, S. Rivera, R. Torrecillas, M. Husband, J. Crossley, I. Robinson, J. Electron. Mater. 43 (2014) 1703–1711.
[12] Y. Kikuchi, T. Nakajo, K. Hayashi, Y. Miyazaki, J. Alloys Compd. 616 (2014) 263–267.
[13] Y. Miyazaki, D. Igarashi, K. Hayashi, T. Kajitani, K. Yubuta, Phys. Rev. B 78 (2008).
[14] T. Yamada, Y. Miyazaki, H. Yamane, Thin Solid Films 519 (2011) 8524–8527.
[15] H. Lee, G. Kim, B. Lee, J. Kim, S.-M. Choi, K.H. Lee, W. Lee, Scr. Mater. 135 (2017) 72–75.
[16] R.B. Song, T. Aizawa, J.Q. Sun, Mater. Sci. Eng. B 136 (2007) 111–117.
[17] G.N. Isachenko, V.K. Zaĭtsev, M.I. Fedorov, A.T. Burkov, E.A. Gurieva, P.P. Konstantinov, M.V. Vedernikov, Phys. Solid State 51 (2009) 1796–1799.
[18] G. Kim, H. Lee, H.J. Rim, J. Kim, K. Kim, J.W. Roh, S.-M. Choi, B.-W. Kim, K.H. Lee, W. Lee, J. Alloys Compd. 769 (2018) 53–58.
[19] G. Skomedal, L. Holmgren, H. Middleton, I.S. Eremin, G.N. Isachenko, M. Jaegle, K. Tarantik, N. Vlachos, M. Manoli, T. Kyratsi, D. Berthebaud, N.Y. Dao Truong, F. Gascoin, Energy Convers. Manag. 110 (2016) 13–21.
[20] W.D. Fei, L.D. Wang, Mater. Chem. Phys. 85 (2004) 450–457.
[21] A. Morozumi, K. Yamada, T. Miyasaka, Y. Seki, 36th IAS Annual Meeting (Cat. No.01CH37248), 3, 2001, pp. 1912–1918.
[22] L. Dupont, Z. Khatir, S. Lefebvre, S. Bontemps, Microelectron. Reliab. 46 (2006) 1766–1771.
[23] U. Scheuermann, P. Beckedahl, 5th International Conference on Integrated Power Electronics Systems, 2008 1–10.
[24] L. DUPONT, Z. Khatir, S. Lefebvre, R. Meuret, B. Parmentier, S. Bontemps, in: EPE 2005 - 11th European Conférence on Power Electronics and Applications, Institute of Electrical and Electronics Engineers - IEEE, Dresde, Germany, 2005, p. 11p.
[25] R. Orrù, R. Licheri, A.M. Locci, A. Cincotti, G. Cao, Mater. Sci. Eng. R. Rep. 63 (2009) 127–287.
[26] L.A. Simpson, T.R. Hsu, G. Merrett, JTE 2 (1974) 503–509.
[27] T.L. Anderson, (2005) 630.
[28] C. Jin, K. Plucknett, Int. J. Refract. Met. Hard Mater. 61 (2016) 151–161.
[29] Y. Feng, T. Zhang, Acta Mech. Solida Sin. 28 (2015) 221–234.
[30] J.J. Kruzic, R.O. Ritchie, J. Am. Ceram. Soc. 86 (2003) 1433–1436.
[31] A.G. Evans, E.A. Charles, J. Am. Ceram. Soc. 59 (1976) 371–372.
[32] G. Roebben, B. Bollen, A. Brebels, J. Van Humbeeck, O. Van der Biest, Rev. Sci. Instrum. 68 (1997) 4511–4515.
[33] A.K. Swarnakar, O.V. der Biest, J.V. Humbeeck, J. Vanhellemont, Phys. Status Solidi C 11 (2014) 1566–1569.
[34] J. Werner, C.G. Aneziris, S. Dudczig, J. Am. Ceram. Soc. 96 (2013) 2958–2965.